

# Energy optimization of a light projection system for buildings that virtually restores artworks

D. VÁZQUEZ,<sup>1</sup> A. A. FERNÁNDEZ-BALBUENA,<sup>1</sup> H. CANABAL,<sup>1</sup> C. MURO,<sup>2</sup> D. DURMUS,<sup>3</sup> W. DAVIS,<sup>3</sup> A. BENÍTEZ,<sup>4</sup> S. MAYORGA,<sup>1,\*</sup>

<sup>1</sup> *Department of Optics, University Complutense of Madrid, Spain*

<sup>2</sup> *Restoration Department, National Museum "Centro de Arte Reina Sofía", Spain*

<sup>3</sup> *The University of Sydney School of Architecture, Design and Planning, Australia*

<sup>4</sup> *Department of Journalism and Audio-visual Communication. Carlos III University of Madrid, Spain*

[\\*smayorga@ucm.es](mailto:smayorga@ucm.es)

**Abstract:** The need to achieve energy efficiency standards in the lighting systems of buildings makes it necessary to optimize all aspects of them. Here, the development of a light projection system that achieves this goal by studying and modifying the spectral output, compared to conventional illumination, is described. A lighting system that estimates the reflectance characteristics of artwork and emits optimized lighting can reduce light absorption. A damage-minimizing point-by-point light projection system is developed using an optimization algorithm, to improve the appearance of the surfaces of artworks whose color has faded. In this case, a simulation of an aged oil painting was made by manipulating the original photograph, which was printed and to which the proposed system was applied. The results show that, when the aged printed image is illuminated with the optimized light source, it appears indistinguishable from the non-aged oil painting.

**Keywords:** Illumination system buildings; virtual restoration; energy optimization.

## Abbreviations

<b>AC:</b> Printed picture .....	5
<b>b:</b> Constant determined in the Berlin model .....	13
<b>CIE:</b> International Commission on Illumination	5
<b>CIEDE2000:</b> Color-difference formula .....	5
<b>DFK-72AUC02-F:</b> CCD Camera.....	16
<b>D<sub>PK</sub>:</b> Real spectral emission projector .....	9
<b>FI<sub>(x,y,rgb)</sub>:</b> Algorithm three-dimensional matrix .....	14
<b>GRF:</b> Global Risk Factor ...	12
<b>H<sub>dm</sub>:</b> Damage factor.....	5
<b>JND:</b> Just-noticeable difference.....	5

<b>K:</b> Adjustment parameter for R, G and B .....	13
<b>L*a*b*:</b> Color space .....	5
<b>LED:</b> Light Emitting Diode ...	4
<b>MF:</b> Merit Function.....	4
<b>P'<sub>PK</sub>:</b> Emitted spectrum from each pixel of the R, G and B channels of the LED projector .....	11
<b>P<sub>cal</sub>:</b> Values corresponding to the amount of RGB of each frame .....	10
<b>PK:</b> Optoma® PK320 RGB LED projector .....	8
<b>S(λ):</b> Relative spectral responsivity.....	13
<b>SPD:</b> Spectral power distribution .....	3
<b>S<sub>PK</sub>:</b> The calculated spectral power distribution of the PK projector.....	8
<b>S<sub>reference</sub>(λ):</b> Spectral power distribution projector with R=G=B=0.5 .....	13

<b>β<sub>1</sub>:</b> Optimized the color differences .....	12
<b>β<sub>2</sub>:</b> Evaluated the damage caused by lighting .....	12
<b>SURF:</b> Speeded up robust feature algorithm.....	16
<b>T:</b> Parameters of the transformation.....	15
<b>w<sub>B1</sub>:</b> weight color difference	13
<b>w<sub>B2</sub>:</b> weight damage function .....	13
<b>Z(λ):</b> Projector factor that relates the spectral measurements with those calculated.....	9
<b>Z:</b> Projector calibration matrix .....	9
<b>ΔE<sub>00</sub>:</b> Minimum color difference with MF .....	12
<b>δ<sub>relative</sub>:</b> Relative light absorption .....	20
<b>ρ<sub>AC</sub>:</b> Printed copies pictures reflectance .....	8

1

## 2 1. Introduction

3 The institutions responsible for cultural heritage are obliged to conserve and exhibit the works of art in  
 4 their collections. The necessary exhibition of artwork causes deterioration due to a variety external agents,  
 5 including inappropriate humidity/temperature (Pavlogeorgatos, 2003) (Mueller, 2013), and optical radiation  
 6 (Michalski, 2013). The former are actually well controlled in museums, damage due to these factors are not  
 7 considered here. The latter, radiation, is controlled in in the ultraviolet (UV) and infrared (IR) wavelength  
 8 ranges with the use of cut-off filters. But the optical radiation in the visible spectrum (380 nm to 780 nm) is  
 9 needed to see the artwork. Radiation causes damage to the artwork through a process called photochemical  
 10 action. When photons are absorbed by a pigment, the energy state of the pigment increases, and its  
 11 chemical composition can change, which produces undesirable effects in paintings, such as the  
 12 discoloration of the paints (Schaeffer 2002). The incident spectral power distribution (SPD), light intensity,  
 13 exposure duration, and sensitivity of the material are four important parameters of photochemical action  
 14 (CIE 2004). While exposure duration and light source intensity have straightforward effects, they are not  
 15 linear (Mayorga, Vazquez et al. 2016).

16 The Berlin model proposes a damage function to quantify the effect of a light source on different types  
17 of artwork (CIE 2004). The damage function takes irradiance (i.e., the intensity of incident radiation) and the  
18 sensitivity of five types of materials (low-grade paper, rag paper, oil paints, textiles, and water colors) into  
19 account. The calculations indicate that radiation of shorter wavelengths causes more damage than longer  
20 wavelengths (Hilbert, Aydinli et al. 1991, CIE 2004). Short wavelength radiation (e.g., UV, blue light) causes  
21 more damage due to the higher energy of the photons, while radiation of longer wavelengths (e.g., IR, red  
22 light) tends to cause damage through radiating heating effects (Cuttle 1996).

23 Saunders and Kirby examined the spectral reflectance functions of different pigments and the damage  
24 caused by optical radiation and found a strong relationship between the spectral reflectance function of a  
25 pigment and damage caused by optical radiation (Saunders and Kirby 1994). For example, damage to red  
26 objects is caused by radiation absorbed in the shorter wavelengths, while blue objects deteriorate due to  
27 the light absorbed in the medium and longer wavelengths. Similarly, Miller proposed that, “the illumination  
28 color should be matched as closely as possible to the reflected color of the artefact,” to prevent the color of  
29 an artwork from fading (Miller 1993). However, matching “illumination color” with “reflected color” would shift  
30 the color appearance of the art (e.g., a red painting would appear very saturated in color under red light).  
31 Therefore, the proposal would work if the illumination color is not “matched with reflected color,” but instead  
32 reverse-engineered to make objects appear the as they do under a reference illuminant, while minimizing  
33 light absorption.

34 A light projection system, that uses sensors to detect object colors (spectral reflectance functions) and  
35 emits spectrally optimized light to reduce the energy absorbed by the artwork, has been proposed (de Luna,  
36 Molini et al. 2015, Durmus and Davis 2015). Investigations focused on architectural applications have shown  
37 that optimizing theoretical test SPDs to minimize the light absorbed by objects can reduce energy  
38 consumption from 38 % to 44 % without altering color appearance (Durmus and Davis 2015). Double-peak  
39 theoretical spectra can further increase energy savings, up to 71 % (Durmus and Davis 2015).  
40 Computational simulations have shown that optimizing spectra to reduce light absorption decreases  
41 damage from 19 % to 47 % for single-color paintings (Durmus, Abdalla et al. 2018). Visual experiments  
42 showed that participants found single-colored real objects under optimized lighting and reference white light  
43 sources to appear equally natural and attractive (Durmus and Davis 2017). Studies have also investigated

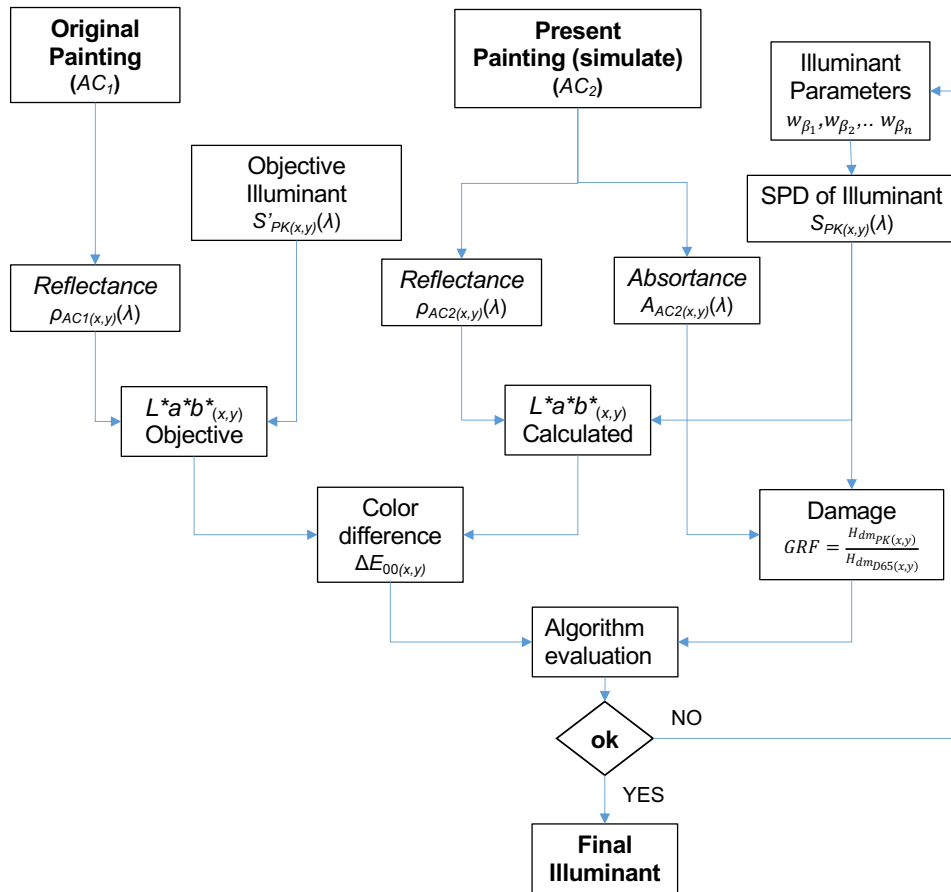
44 the use of optimized lighting systems, including daylight and LED applications, in museums to save energy  
45 and, therefore, help reduce energy dependence and pollution (De-Graaf, Mennatalla et al. 2013, Mueller  
46 2013, Mayorga, Vazquez et al. 2016, Al-Sallal, AbouElhamd et al. 2018).

47 Other researchers have used spectral optimization methods to reduce damage to artwork (Berns 2011,  
48 Delgado, Dirk et al. 2011) and restore the faded colors of museum artefacts (Viénot, Coron et al. 2011) by  
49 illuminating them with customized spectra. With some new techniques, art conservators can use light to  
50 restore the faded appearance of a masterpiece to its original state, as was done for Rothko's painting (Hecht  
51 2015). projecting the original color of the painting, which was obtained thanks to the existence of slides of  
52 the original. This was done by projecting the original (non-faded) color of the painting, which was obtained  
53 from slides of the original. A projection system projects a compensation image on the original canvas to  
54 obtain a restored color appearance (Stenger, Khandekar et al. 2016). Berns used spectral calculations to  
55 create adjustment curves, where segmented portions of an object's image were translated in color (Berns  
56 2019). The absorption-minimization concept can be applied to museum lighting to reduce damage to  
57 sensitive materials, as well as to restore the appearance of already-damaged artwork.

58 Here, the construction of a point-by-point light projection system is described and its abilities to reduce  
59 damage from optical radiation and maintain the color quality of a multi-colored painting are quantified. The  
60 presented work is based, therefore, on the metamerism colors, which are colors that appear the same to a  
61 human observer but have different SPDs (Schanda 2007).

## 62 **2. Methods**

63 The system developed in this work consists in the characterization and processing of the spectral  
64 reflectance of the artwork in its current state and in its objective state to be achieved, so that the system  
65 can recover its color and control damage point by point. The following flow diagram (Fig. 1) the optimization  
66 process is described, from the characterization of the paint until obtaining better final illuminant for  
67 reconstruction and lighting of the same, causing the least possible damage.



68

69

**Fig. 1. Flow diagram**, the steps of the optimization process for obtaining better final illuminant are described.

70

71

72

73

74

75

76

77

78

79

80

A prototype of the point-by-point light projection system has been constructed using a calibrated red-green-blue (RGB) projector, multispectral filters and a computer system. A multispectral imaging camera was used to recover the spectral reflectance function of an oil painting reproduced in a printed copy derived from a photograph. An RGB projector was calibrated to emit light to each pixel of the printed picture, that depicts an aged version of the painting, using an optimization algorithm and a merit function (MF) to develop a light projection system that is capable of:

- *Obtain a good color quality of the printed picture*: The appearance of color between the printed copy illuminated with an International Commission on Illumination (CIE) daylight D65 reference and the printed copy color visually restored with the daylight projection system must be minimal. The reference illuminant D65 was used because it represents daylight at 6500 K which represents the lighting conditions where the painter created the artwork (Phillips 1912). The color difference ( $\Delta E_{00}$ )

81 was calculated in CIE 1976  $L^*a^*b^*$  using the CIEDE2000 formula (CIE 2004), because the formula  
82 provides an improved estimation of industrial color differences (G. Sharma 2005) where  $\Delta E_{00}=1$  is  
83 a just-noticeable difference (JND) under controlled laboratory conditions (Fechner 1860, Fairchild  
84 2013).

85 - *Reduce damage of the artworks*: The Berlin model (CIE 2004), which determines the damage  
86 caused to different materials ( $H_{dm}$ ) from the spectral irradiance of illumination, was used to minimize  
87 the damage caused by optical radiation. Damage factor ( $H_{dm}$ ) depends on the SPD and radiant flux  
88 of the illuminant, as well as the responsivity of the illuminated material.

### 89 **2.1 Color difference of the printed copies of picture**

90 In this research, a digital archival image of Joaquín Sorolla's painting, "*Walk on the beach*", 1909  
91 (provided by the Sorolla Museum Foundation inv. 834), was used to generate two printed copies, as shown  
92 in Fig. 2(a) and 2(b). They were printed with a Xerox 550 color printer with the same characteristics.

93 The digital archive was digitally changed with a filter using MATLAB® to simulate the photochemical  
94 aging process caused by light radiation, corresponding to  $AC_2$  as shown in Fig. 2(b). The printed copy  $AC_1$   
95 is the digital archive given by the Sorolla Museum and served as a control to simulate an ideal color  
96 characteristic of the painting as shown in Fig 2(a).

97 The aim of this investigation is to illuminate the printed copy  $AC_2$  with the light projection system  
98 developed such that it has the color appearance of the undamaged  $AC_1$ . The goal is to demonstrate that,  
99 following a certain method and with the necessary information about the color and reflectance of the artwork,  
100 a light projection system can be developed that, when applied to real artwork, minimizes the damage and  
101 improves the color appearance. Fig. 2(c) shows the CIE 1976  $L^*a^*b^*$  coordinates calculated for each of the  
102 printed copies when illuminated by D65 illuminant.

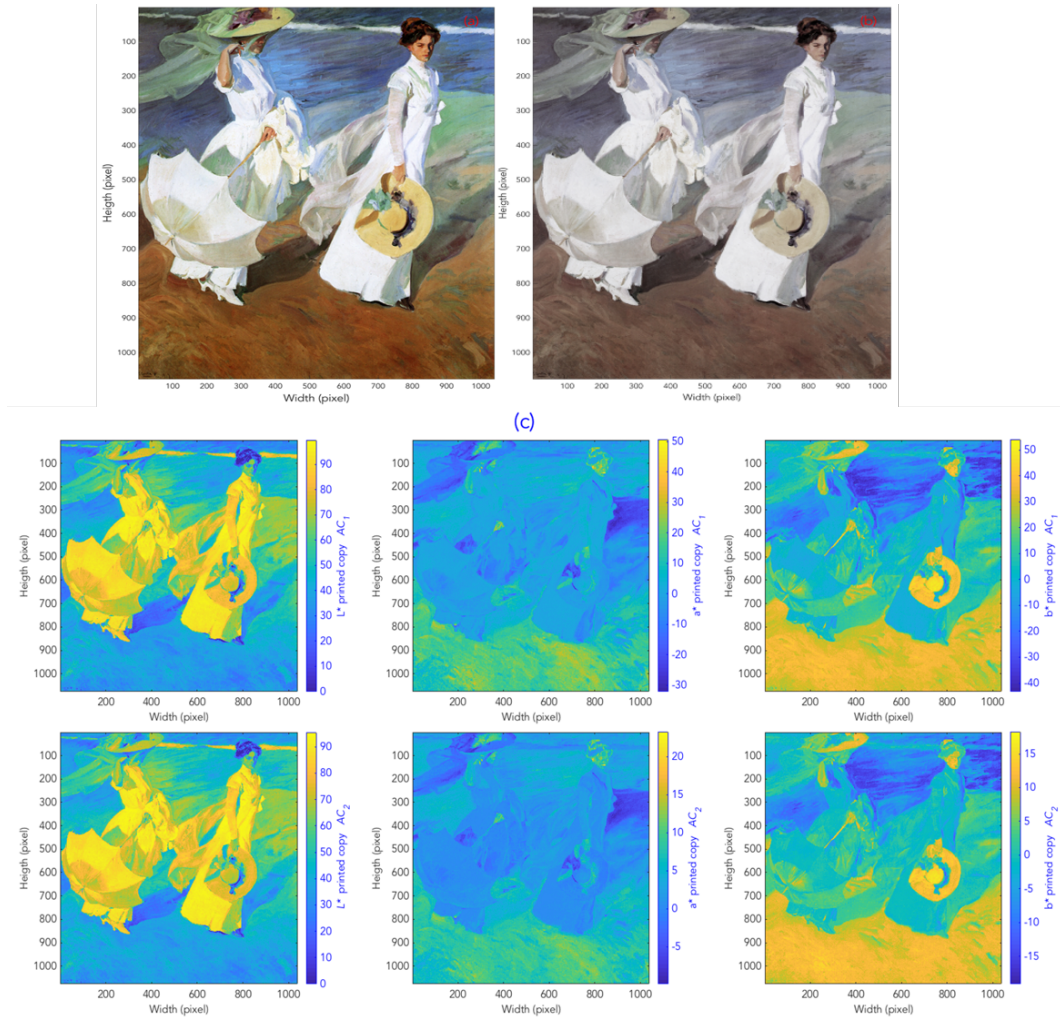
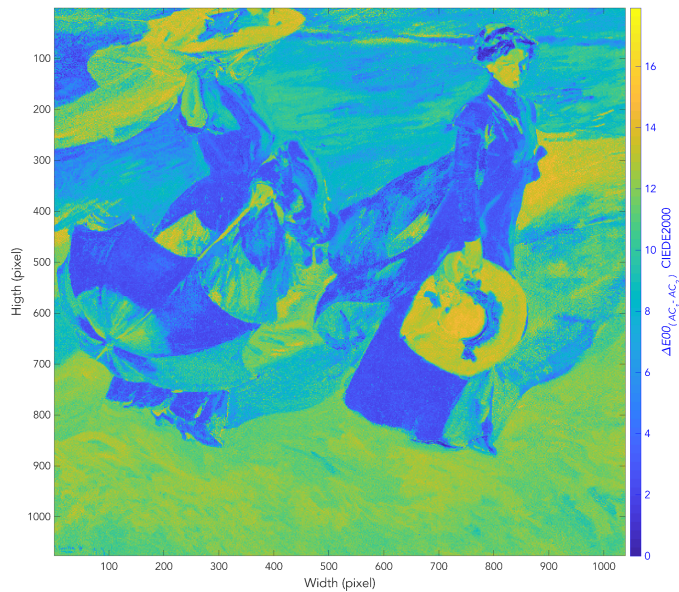


**Fig. 2. "Walk on the beach" printed copies** (a) The printed copy that simulates the reference painting was recovered from a digital archive courtesy of the Sorolla Museum Foundation inv. 834 ( $AC_1$ ), (b) the digital archive ( $AC_1$ ) was modified to appear faded using MATLAB® and was printed ( $AC_2$ ). (c) Calculated color space coordinates ( $L^*a^*b^*$ ) corresponding to the two images described in Fig. 2(a) and Fig. 2(b).

103  
104  
105  
106  
107

108 The  $L^*a^*b^*$  values were used to calculate the differences in color between the two images, to achieve  
109 the desired aging effect. The color difference created between the two printed pictures was such that the  
110 difference would be clearly noticeable to an observer ( $1.0 < \Delta E_{00} < 20$ ). The color difference  $\Delta E_{00}$  between the  
111 two printed copies was calculated with CIEDE2000, obtaining the values shown in Fig. 3. The average value  
112 was  $\Delta E_{00} = 8.85$ .



113

114

115

**Fig. 3. CIEDE2000  $\Delta E_{00}$ .** Image shows color differences between the two printed pictures,  $AC_1$  and  $AC_2$ , before applying the developed light projection system.

116

## 2.2 Spectral characterization of the printed pictures

117

118

119

120

121

122

In artwork conservation, the original work of art is generally used to determine differences in the spectral reflectance functions between the original object and reproductions, and to provide more accurate spectral reflectance estimation (Imai, Rosen et al. 2000). When the original painting cannot be used as a reference, which is common in the case of old paintings, other techniques can be used to measure the reflectance function, such as restoring or cleaning selected small areas (Hwang, Song et al. 2017) and characterizing the artwork by old photographic records (Stenger, Khandekar et al. 2016).

123

124

125

126

127

128

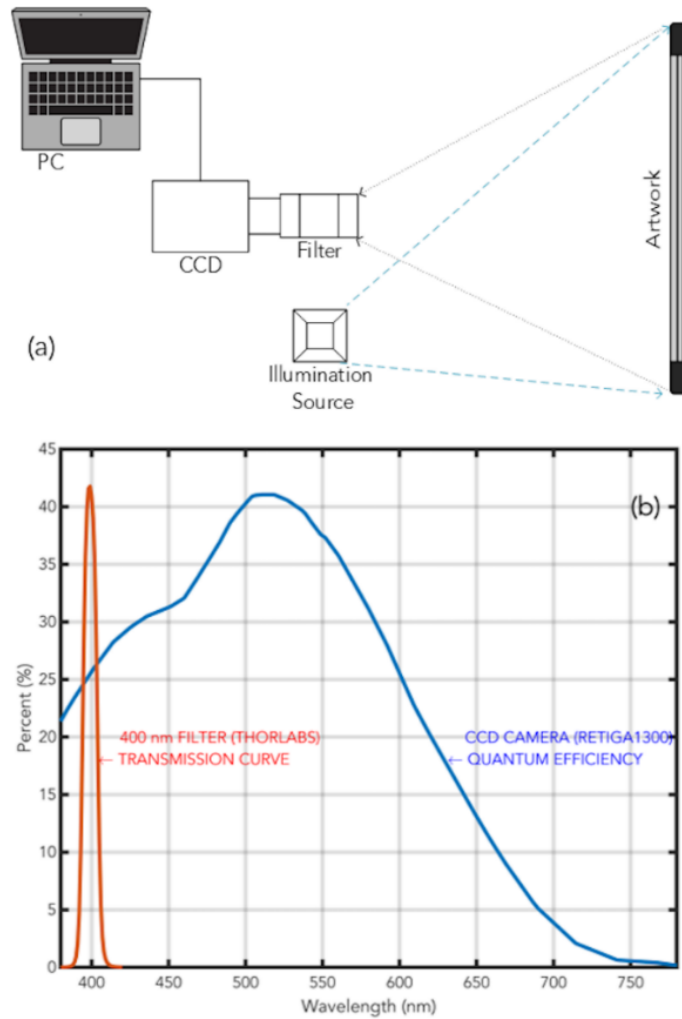
129

130

131

The spectral reflectance factors of the printed pictures ( $AC_1$  and  $AC_2$ ) were measured using high resolution monochromatic multispectral images (Shen, Cai et al. 2007, Murakami, Yamaguchi et al. 2012, Chane, Mansouri et al. 2013). Fig. 4(a) shows a diagram of the elements used for the acquisitions of multispectral images. Twenty multispectral images were taken with a QIMAGING® Retiga 1300 CCD high-resolution camera, which is sensitive in the visible spectral range, as shown in Fig. 4(b). Each monochromatic image captured a different spectral range, since twenty multispectral Thorlabs® band-pass filters were placed in front of the camera, each with a full width at half maximum of  $10 \text{ nm} \pm 2 \text{ nm}$ . The first image was captured with a 400 nm filter FB400-10, (i.e., the maximum transmittance of the second filter was at 420 nm FB420-10, and so on) up to 780 nm (FB780-10). In Fig. 3(b) the spectral behavior of the 400

132 nm filter with respect to visible radiation is shown as an example of the filters used. The lighting source was  
 133 a standard 100 W Philips incandescent lamp, placed in front of the printed picture at a 45° angle relative the  
 134 central axis of the system.



135  
 136 **Fig. 4 Spectral characterization** (a) Multispectral images of the printed pictures were taken with a QIMAGING®  
 137 Retiga 1300 CCD camera and 20 Thorlabs® filters, with peak spectral transmittances from 400 nm to 780 nm.  
 138 Printed pictures were illuminated with a lamp with spectral emission similar to CIE illuminant A (incandescent  
 139 lamp), and computer software was used to record measurements and process data. (b) The spectral sensitivity  
 140 of the QIMAGING® Retiga 1300 CCD camera and transmission characteristics of the Thorlabs® filter. The  
 141 spectral transmission function shown in the graph corresponds to one of the filters used, with peak transmittance  
 142 at 400 nm.

143 The spectral reflectance of each pixel,  $\rho_{AC(x,y)}(\lambda)$  was acquired for  $AC_1$  and  $AC_2$  from 20 multispectral  
 144 images. The size of each reflectance factor array of the multispectral image of the picture ( $\rho_{AC1(x,y)}(\lambda)$ ,

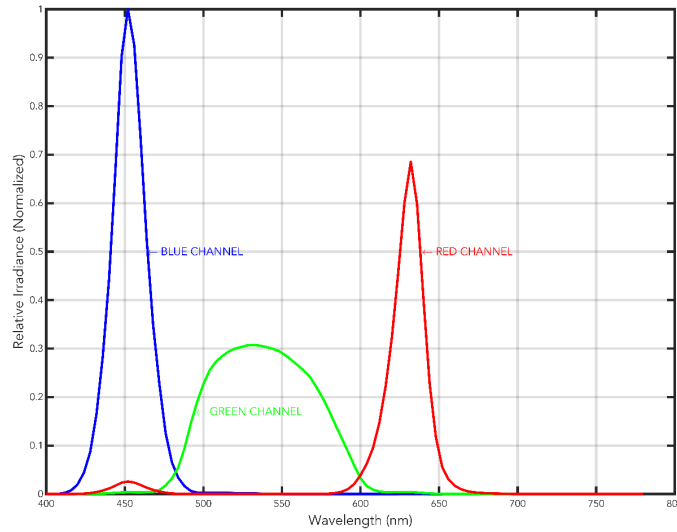
145  $\rho_{AC_2(x,y)}(\lambda)$  was  $x=411$  pixels and  $y=450$  pixels. The image size (174.9 mm x 273.6 mm) corresponded to  
 146 pixels with dimensions of 0.608 mm x 0.425 mm.

### 147 2.3 Projector calibration

148 An Optoma® PK320 RGB LED projector (PK) was used to illuminate the artificially aged printed picture  
 149 ( $AC_2$ ) to virtual restore its appearance ( $AC_1$ ). The calculated spectral power distribution of the PK projector,  
 150  $S_{PK(x,y)}(\lambda)$ , for each pixel of the aged printed copy ( $AC_2$ ) was

$$151 \quad S_{PK(x,y)}(\lambda) = K_{R(x,y)} R_{PK}(\lambda) + K_{G(x,y)} G_{PK}(\lambda) + K_{B(x,y)} B_{PK}(\lambda), \quad (1)$$

152 where  $R_{PK}(\lambda)$ ,  $G_{PK}(\lambda)$ ,  $B_{PK}(\lambda)$  are the SPDs of the red, green and blue channels of the PK, as shown in Fig.  
 153 5, and  $K_{R(x,y)}$ ,  $K_{G(x,y)}$ ,  $K_{B(x,y)}$  are intensity adjustment parameters ranging from 0.0 to 1.0.



154  
 155 **Fig. 5. Spectral curves of the Optoma® PK320 projector.** The spectral power distribution of the RGB  
 156 channels of the PK projector at their maximum intensities:  $R_{PK}(\lambda)$  when  $K_R=1.0$  for the red channel,  $G_{PK}(\lambda)$  when  
 157  $K_G=1.0$  for the green channel, and  $B_{PK}(\lambda)$  when  $K_B=1.0$  for the blue channel. To obtain the SPD of the projector,  
 158 a fixed image of each color was projected onto a diffuse white screen with a measured reflectance of 95%. The  
 159 measurements were obtained with a Photo Research SpectraScan® Spectroradiometer PR655.

160 Since the calculated SPD,  $S_{PK(x,y)}(\lambda)$ , was not identical to the real spectral emission of the PK,  $D_{PK(x,y)}(\lambda)$ ,  
 161 the projector was calibrated using a linear least-squared error approximation model to equate  $S_{PK(x,y)}(\lambda)$  with  
 162  $D_{PK(x,y)}(\lambda)$ . Since a spectral, rather than colorimetric, calibration is required for this study, the calibration  
 163 process differs from that usually employed for projectors and display screens (Simpson and Jansen 1991,  
 164 Marimont and Wandell 1992, Quiroga, Zoido et al. 1994). These models propose the following relationship  
 165 between the output and input signal

166

$$D_{PK(x,y)}(\lambda) = Z(\lambda) S_{PK(x,y)}(\lambda), \quad (2)$$

167

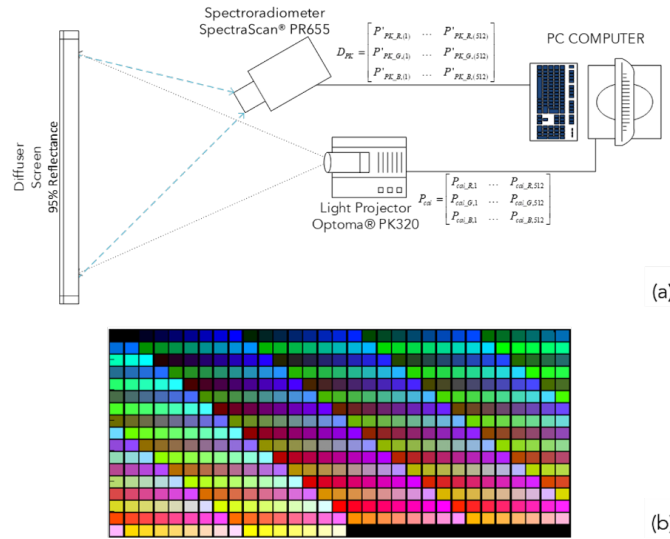
where  $Z(\lambda)$  is a dimensionless factor that relates the spectral measurements with those calculated.  $PK$  was

168

been calibrated to calculate  $Z$ . Fig. 6(a) shows the diagram of the elements used for the calibration of the

169

$PK$ .



170

171

**Fig. 6. Diagram of the calibration equipment and process.** (a) A diffuse white screen with 95 % reflectance, a

172

Photo Research SpectraScan® Spectroradiometer PR655 and a computer were used to calibrate the RGB

173

Optoma® PK320 projector, and (b) an array of 512 pixels.

174

An array of 512 pixels, shown in Fig. 6(b), was composed of a combination of different RGB values to

175

covers the widest possible color gamut. An array, with a size of 512 x 3 pixels,  $P_{cal}$ , was formed

176

$$P_{cal} = \begin{bmatrix} P_{cal,R,(1)} & \dots & P_{cal,R,(512)} \\ P_{cal,G,(1)} & \dots & P_{cal,G,(512)} \\ P_{cal,B,(1)} & \dots & P_{cal,B,(512)} \end{bmatrix}, \quad (3)$$

177

where  $P_{cal\_R1...512}$  were the values corresponding to the amount of red (R) of each frame,  $P_{cal\_G1...}$  were the

178

green (G) values and  $P_{cal\_B1...B512}$ , were the blue (B) values.

179

The array  $P_{cal}$  was projected on to a white screen with  $PK$ . Using the Photo Research SpectraScan®

180

Spectroradiometer PR655, 512 non-contact measurements were made at each point of each projected

181

frame. These values were corrected, by taking the spectral reflectance function of the screen

182

( $\rho_{screen\_diffuser}=0.95$ ) into account, and the resulting values were the spectral emission of the projector for

183 each frame,  $D_{PK}(\lambda)$ , which, for the calibration calculations, was divided into the three emission channels of  
 184 the projector, R, G and B, independently.

$$185 \quad P'_{PK_R(1,\dots,512)}(\lambda) = D_{PK_R(1,\dots,512)}(\lambda) R_{PK}(\lambda), \quad (4)$$

$$186 \quad P'_{PK_G(1,\dots,512)}(\lambda) = D_{PK_G(1,\dots,512)}(\lambda) G_{PK}(\lambda), \quad (5)$$

$$187 \quad P'_{PK_B(1,\dots,512)}(\lambda) = D_{PK_B(1,\dots,512)}(\lambda) B_{PK}(\lambda), \quad (6)$$

188 where  $P'_{PK_R(1,512)}(\lambda)$ ,  $P'_{PK_G(1,512)}(\lambda)$  and  $P'_{PK_B(1,512)}(\lambda)$  represent the spectrum emitted by from each pixel of  
 189 the red, green and blue channels of the LED projector, respectively.  $D_{PK}(\lambda)$  is the sum of the spectral values  
 190 measured for each channel and for each frame

$$191 \quad D_{PK(1,\dots,512)}(\lambda) = P_{PK_R(1,\dots,512)}(\lambda) + P_{PK_G(1,\dots,512)}(\lambda) + P_{PK_B(1,\dots,512)}(\lambda). \quad (7)$$

192 The measured values (spectral data of each frame) and the calculated values ( $R$ ,  $G$  and  $B$  data of each  
 193 frame) were unified in the same dimensional space to characterize the relationship between them ( $Z$ ). The  
 194 spectral values from equations 4, 5 and 6 were transformed to  $R$ ,  $G$  and  $B$  tristimulus values ( $P'_{PK_R(n)}$ ,  
 195  $P'_{PK_G(n)}$ ,  $P'_{PK_B(n)}$ ) using the CIE 1931 standard observer (CIE 2004, Schanda 2007). As a result,  $D_{PK}$  can  
 196 be expressed as a 512 x 3 element array of RGB values

$$197 \quad D_{PK} = \begin{bmatrix} P'_{PK_R(1)} & \dots & P_{cal_R(512)} \\ P'_{cal_G(1)} & \dots & P_{cal_G(512)} \\ P'_{cal_B(1)} & \dots & P_{cal_B(512)} \end{bmatrix}, \quad (8)$$

198 where,  $P'_{PK_R(1)\dots(512)}$ ,  $P'_{PK_G(1)\dots(512)}$  and  $P'_{PK_B(1)\dots(512)}$  are the  $R$ ,  $G$  and  $B$  values of each pixel (1 to 512).

199  $D_{PK}$  and  $P_{cal}$  were used to calculate the projection system's deviation from the input signal employing the  
 200 least squares adjustment of the linear transformation (Quiroga, Zoido et al. 1994)

$$201 \quad D_{PK} = ZP_{cal}, \quad (9)$$

202 where  $Z$  is a 3 x 3 matrix that solves the RGB deviation of the  $PK$  for each pixel of the output signal.

203 Matrix  $Z$  was obtained by the least squares' adjustment

$$204 \quad \hat{Z} = (P_{cal}P_{cal}^T)^{-1}P_{cal}^TD_{PK}, \quad (10)$$

205 and the values obtained from the calibration of the projection system were

206

$$\hat{Z} = \begin{bmatrix} 0.8955 & -0.1972 & 0.0688 \\ -0.1306 & 0.9272 & -0.1078 \\ 0.0615 & -0.0342 & 0.9039 \end{bmatrix}, \quad (11)$$

207

208

209

In order to check the validity of the adjustment, the mean squared error (MSE) of the calibration model for each channel ( $\mathcal{E}_R=0.0371$ ,  $\mathcal{E}_G=0.0358$ , and  $\mathcal{E}_B=0.0665$ ), and their standard deviations ( $\sigma_R=0.0021$ ,  $\sigma_G=0.0043$ , and  $\sigma_B=0.0021$ ) were calculated.

210

#### 2.4 Merit function

211

212

213

214

215

216

A merit function (MF) is a weighted combination of minimization objectives (i.e., parameters to be minimized) in multi-objective optimizations. Here, a dynamic MF (Fernandez-Balbuena, Gonzalez et al. 2015) was applied to optimize the lighting parameters (color appearance of artificially aged printed picture and damage factor). Considering the major influence that the illuminant has on the appreciation of color in the exhibition of art, it was necessary to minimize the difference in color appearance between the reference and the test lighting conditions. The MF ( $\beta_1$ ) optimized the color differences, CIEDE2000  $\Delta E_{00(x,y)}$  (CIE 2004)

217

$$\beta_1 = \Delta E_{00(x,y)} = \sqrt{\left(\frac{\Delta L'}{K_L S_L}\right)^2 + \left(\frac{\Delta C'}{K_C S_C}\right)^2 + \left(\frac{\Delta H'}{K_H S_H}\right)^2 + R_T \left(\frac{\Delta C'}{K_C S_C}\right) \left(\frac{\Delta H'}{K_H S_H}\right)}, \quad (12)$$

218

219

220

221

where  $\Delta L'$ ,  $\Delta C'$  and  $\Delta H'$  are the differences the lightness ( $L'$ ), chroma ( $C'$ ) and hue ( $H'$ ) between the coordinates of a pixel in the printed pictures under the reference condition (D65 illuminant) and test condition (optimized lighting). The values obtained from the reflectance of printed pictures,  $\rho_{AC}(\lambda)$ , were transformed using CIEDE2000, and the MF created iterations until a minimum  $\Delta E_{00}$  was obtained.

222

223

224

225

226

227

In addition to color difference, another MF ( $\beta_2$ ) evaluated the damage caused by lighting. In this model a numerical measured standard value is used, the Global Risk Factor (GRF) (Mayorga, Vazquez et al. 2016), which compares the D65 illuminant and the PK illumination system in a way that is easy to interpret. The value obtained for the GRF indicates the number of times that the damage to the illuminated area equals or exceeds the damage caused by the D65 illuminant, with a value of unity for areas having the same damage factor ( $H_{dm}$ ).

228

$$\beta_2 = GRF = \frac{H_{dm\_PK(x,y)}}{H_{dm\_D65(x,y)}}, \quad (13)$$

229

230

where GRF is dimensionless, and  $H_{dm\_PK}$  is the effective radiant exposure of the projector and  $H_{dm\_D65}$  is the effective radiant exposure of the D65 illuminant, in  $\text{Whm}^{-2}$ .

231 
$$H_{dm_{PK}(x,y)} = \iint_{\lambda,t} E_{PK}(\lambda)(t) S(\lambda) A_{PK,x,y}(\lambda) d(\lambda) d(t), \quad (14)$$

232 
$$H_{dm_{D65}(x,y)} = \iint_{\lambda,t} E_{D65}(\lambda)(t) S(\lambda) A_{D65,x,y}(\lambda) d(\lambda) d(t), \quad (15)$$

233 where  $E(\lambda)$  is the spectral irradiance of the incident light, in  $\text{Wm}^{-2}$ , on each pixel  $(x, y)$  for D65 or PK,  $A(\lambda)$  is  
 234 the absorbance function for each illuminant for each pixel  $(x, y)$  of the printed picture and  $S(\lambda)$  is the relative  
 235 spectral responsivity of the painting normalized a 300 nm, represented by an exponential function of the  
 236 form

237 
$$S(\lambda) = \exp[-b(\lambda - 300)], \quad (16)$$

238 where  $b=0.0115$  for oil paints on canvas (CIE 2004). Although the picture used here is printed on paper, the  
 239 oil paint sensitivity data are used, since the aim of the research is to eventually used this method to reduce  
 240 damage to real works of art.

241 When the two objective functions are combined, the final MF is expressed as

242 
$$MF = (w_{\beta_1}\beta_1 + w_{\beta_2}\beta_2), \quad (17)$$

243 where  $w_{\beta_1}$  and  $w_{\beta_2}$  are weights ranging from 0.0 to 1.0.  $\beta_1$  and  $\beta_2$  are optimized separately, to minimize their  
 244 values as much as possible. The optimization is conditioned by the weights ( $w_{\beta_1}$  and  $w_{\beta_2}$ ) assigned to each  
 245  $\beta$ . The MF results determines when the calculation stops. The freedom of being able to modify the weights  
 246 to give more importance to one of the factors (damage or color difference) provides flexibility to this  
 247 methodology.

## 248 **2.5 Optimization algorithm**

249 A Nelder-Mead simplex algorithm (Nelder and Mead 1965) was used to optimize the color appearance  
 250 and minimize damage caused by optical radiation. This optimization method, based on the simplex concept  
 251 (Lagarias, Reeds et al. 1998), is a technique commonly used to minimize a multi-objective function, and it  
 252 has been shown to be a suitable method for the optimization of lighting systems (Lin, Huang et al. 2013).

253 The algorithm calculated the optimal spectral power distribution and the intensity of each point in the  
 254 image  $S_{AC(x,y)}(\lambda)$ . These values result from adjusting the  $K$  parameters ( $K_R$ ,  $K_G$ , and  $K_B$ ) described in Eq. (1).  
 255 The calculation started with  $S_{reference}(\lambda)$ , which was defined as  $K_R=0.5$ ,  $K_G=0.5$  and  $K_B=0.5$ .  $K$  values were  
 256 changed in different sequences, which did not influence the result. The optimization terminated when

257 optimal values for each pixel were reached, the predefined maximum iterations were reached, the constraint  
258 functions could not be reduced any further, or the end of the sequence was reached.

## 259 **2.6 Optimization of lighting**

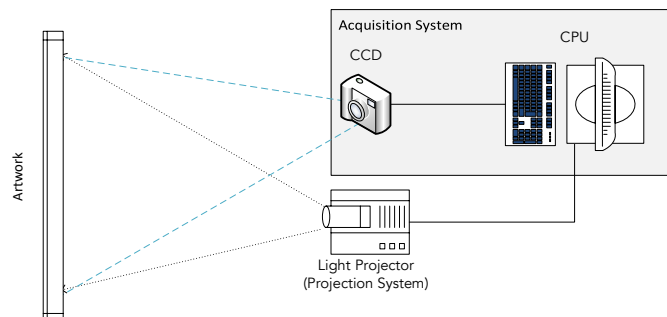
260 The calculated light emission of the projector is an optimized value, with the merit function of the  $K$   
261 parameters ( $K_R$ ,  $K_G$ , and  $K_B$ ) for the selected pixel that, when the spectral profile of the  $PK$  projector is  
262 applied, produces a light emission that causes minimal damage and minimal color difference between the  
263 aged and non-aged printed pictures. The final values of the  $K$  parameters ( $K_R$ ,  $K_G$ , and  $K_B$ ) are the R, G and  
264 B of each pixel.

## 265 **2.7 Lighting projection**

266 The optimized lighting calculated by the algorithm is a three-dimensional matrix,  $Fl_{(x,y,rgb)}$ , where the third  
267 dimension represents the intensities of the  $R$ ,  $G$  and  $B$  channels of the projector. The spatial coordinates ( $x$ ,  
268  $y$ ) correspond to the reference system defined by the position and spectral reflectance obtained by  
269 multispectral imaging.

270 Since the projector had to be positioned slightly off-axis to the printed copy picture, the projected image  
271 was expected to be distorted due to the change of perspective (i.e., keystone effect), as well as the  
272 difference in the optical characteristics of the acquisition and projection systems (i.e., focus, magnification  
273 and optical distortions).

274 In theory, it is possible to accurately determine the position, orientation and optical characteristics of the  
275 artwork, acquisition system and projector, as shown in Fig. 7. These aspects (position, orientation and  
276 optical characteristics) are necessary to pre-calculate the inverse transformation function that compensates  
277 for all deformations and distortions. However, this would impose extremely strict experimental requirements  
278 in terms of the accuracy of the measurements and the stability of the system.



279

280 **Fig. 7. Diagram of the light projection system**, consisting of a printed picture, an image acquisition system (a  
281 CCD camera and a PC), and a projector. Images were taken with the CCD camera and were spatially tested  
282 using the software developed by the researchers. The signal was adjusted in real time, so that the light was  
283 always focused on the surface of the illuminated printed picture.

284 To avoid these strict requirements, a calibration method was developed based on triangulation  
285 techniques to infer the geometric parameters of all the elements by projecting circular beams of light. The  
286 system was inspired by structured light projection techniques where the correspondences between the  
287 projected light patterns and their images are characterized, also known as the correspondence problem in  
288 computer vision (Capel and Zisserman 2003). An added difficulty was that, in the projection plane there was  
289 an object with a variable reflectance distribution, which complicated the detection and automatic indexing  
290 of the projected structures and prevented the use of the traditional chessboard pattern. Therefore, a  
291 temporal modulation pattern was projected for identification and labeling. This process requires additional  
292 processing time but increases the accuracy of the calibration using sub-pixel precision techniques (Bouquet  
293 2012).

294 Using the MATLAB<sup>®</sup> image processing toolbox, the coordinates of the centroids of the projected patterns  
295 in the projection plane  $(x_p, y_p)$  and the parameters of the transformation  $T$  were obtained. The data were  
296 used to establish the correspondence with the array of the projected theoretical positions  $(x, y)$ . The  
297 transformation  $T$  was obtained by a two-stage process. First, an approximate initial estimate was generated,  
298 in which a projective transformation was assumed (straight lines remain straight, and parallel lines converge  
299 towards a vanishing point). Subsequently,  $T$  was refined with a polynomial adjustment, which accounted for  
300 possible distortions introduced by the optical systems (Zhang 2000). The inverse transformation,  $T^{-1}$ , was  
301 applied to the optimized lighting condition,  $S'_{AC(x,y)}(\lambda)$ , so that the projected image was  $T^{-1}[S_{AC(x,y)}(\lambda)]$ , and  
302 the resulting signal became  $S'_{AC(x,y)}(\lambda)$ .

303 The estimation of the transformation,  $T$ , was used to correct the distortions in the three-dimensional  
304 composition formed by the projector, the camera and the printed picture. However, the origin coordinates  
305 acquired by the spectroradiometer must be precisely matched with the specific position of the printed  
306 pictures in the projection plane.

307 Manual adjustments were omitted for greater precision in the process, and artificial vision techniques,  
308 based on the search for correspondence between pairs of images (Vincent and Laganière 2005), were used

309 to detect the exact position of the printed pictures. An additional advantage of this process is the automatic  
310 readjustment of the system, which allows maintenance of the printed picture and the exhibition space. An  
311 algorithm called the speeded up robust features (SURF) detector (Bay, Ess et al. 2008) was used to detect  
312 and describe the points of interest of an image, which has a good sensitivity to position and scale changes.

313 Once the most relevant points of interest were detected, they were paired based on the similarity of the  
314 detected characteristics, while pairs that did not exceed predetermined threshold limits were discarded.

315 The control of the position of the printed pictures and the projector was carried out by a DFK-72AUC02-  
316 F Imaging Source CCD camera, as shown in Fig. 8. The camera has an autofocus function and spatial  
317 resolution of 2592 x 1944 pixels. It transferred the information to a mini PC, which ran the artificial vision  
318 algorithm. With this artificial vision algorithm, it was possible to obtain accurate positioning of the image  
319 within 0.5 pixels. Software was developed for the proposed practical example, which analyzed and  
320 performed corrections.



321

322 **Fig. 8. Proposed light projection system**, consisting of the Optoma® PK320 projector, that emits light onto of  
323 the painting, a DFK-72AUC02-F CCD camera, which was used to correct the spatial position of the system with

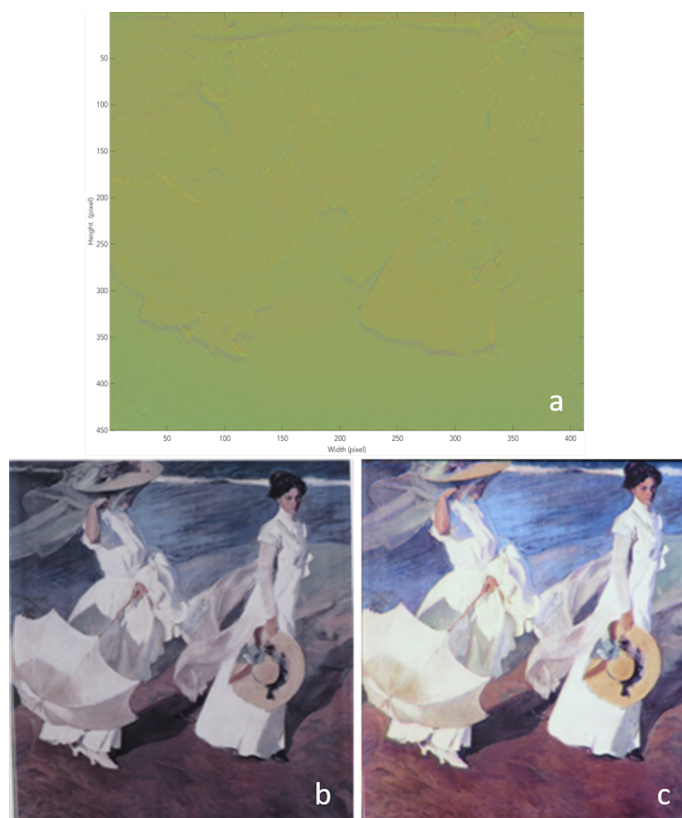
324 respect to the illuminated printed picture, and the PC that processes the CCD data and applies the artificial  
325 vision algorithm to correct the image emitted by the projector according to the location of the printed picture.

### 326 3. Results

327 The light projection system optimized the lighting from the RGB projector to minimize the color difference  
328 between the reference photography and restored printed copy picture. The light absorption and the color  
329 quality of the printed copy picture under D65 illuminant and optimized lighting were quantified.

#### 330 3.1 Optimized lighting emitted by the projector to the printed picture AC<sub>2</sub>.

331 The values obtained for the R, G and B of each pixel are represented in Fig. 9(a). The damage and color  
332 resulting from the light emitted by the light projection system depends on the R, G and B values obtained  
333 with the merit function, the spectral profile of the projector, the calibration of the projector and the lighting  
334 projection. Through these processes, non-invasive virtual photonic restoration was carried out to improve  
335 the appearance of the artificially aged printed image, as shown in Fig. 9(b), achieving a visual recovery of  
336 the color without physical intervention, as shown in Fig. 9(c).



337  
338 **Fig. 9. Virtual photonic restoration** (a) Shows the RGB value obtained with the merit function. With these RGB  
339 values, the artificially aged printed material has a minimum color difference and the damage is optimized (non-

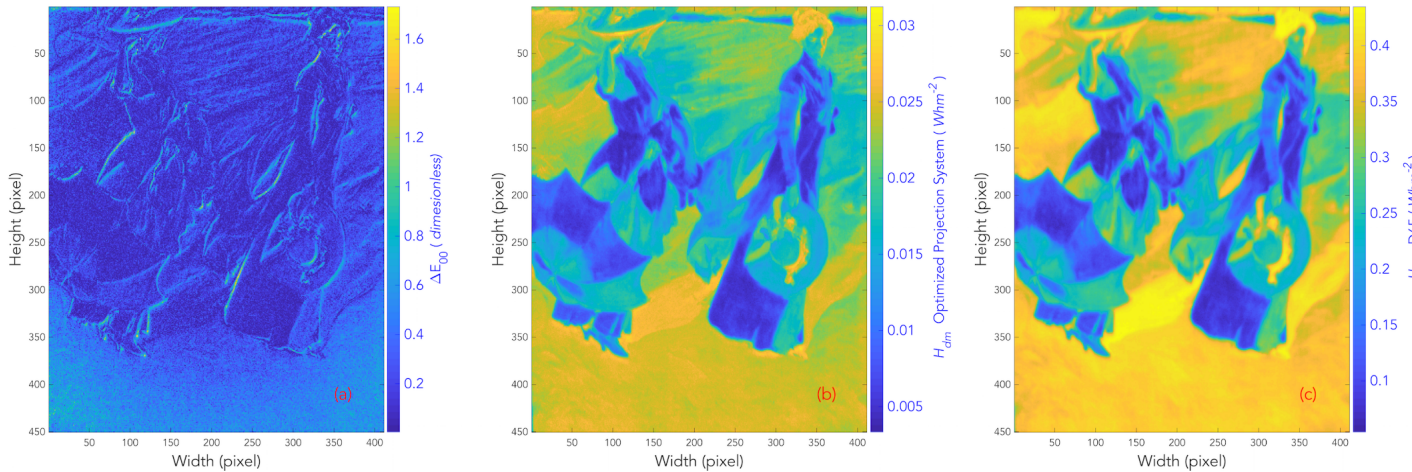
340 invasive virtual photonic restoration method). (b) The spatially and spectrally optimized lighting can enhance the  
 341 color appearance of a faded printed picture shows  $AC_2$  with artificial aging (c) shows the color appearance of  
 342  $AC_2$  with the application of the non-invasive virtual photonic restoration method.

### 343 3.2 Minimization of color difference and damage obtained with the merit function

344 The results obtained with the merit function improved the performance of light projection system by  
 345 approaching the ideal composition of reflected light to restore the appearance of the artificially aged printed  
 346 picture. The resulting color differences for each pixel between the original printed picture  $AC_2$  and the  
 347 artificially damaged printed picture  $AC_2$  when illuminated by optimized test lighting ( $\Delta E_{00(x,y)}$ ) are shown in  
 348 Fig. 10(a). The average color difference suggests that the printed picture  $AC_2$  would appear indistinguishable  
 349 under the optimized lighting condition from printed picture  $AC_1$  when illumination by the reference lighting  
 350 condition. However, in 458 pixels (less than 0.25 % of the image), the color difference was greater than 1.0.

351 Fig. 3 compares the appearance of between the two printed pictures ( $AC_1$  and  $AC_2$ ) when both are  
 352 illuminated by D65, with an average color difference between the images of  $\Delta E_{00}=8.85$ . With the MF  
 353 optimization, the color difference between  $AC_1$  and “ $AC_2$  restored,” as shown in Fig. 9(c), is  $\Delta E_{00(x,y)}=0.27$ .  
 354 As shown in Fig. 10(a), the average color difference has been reduced 33 times.

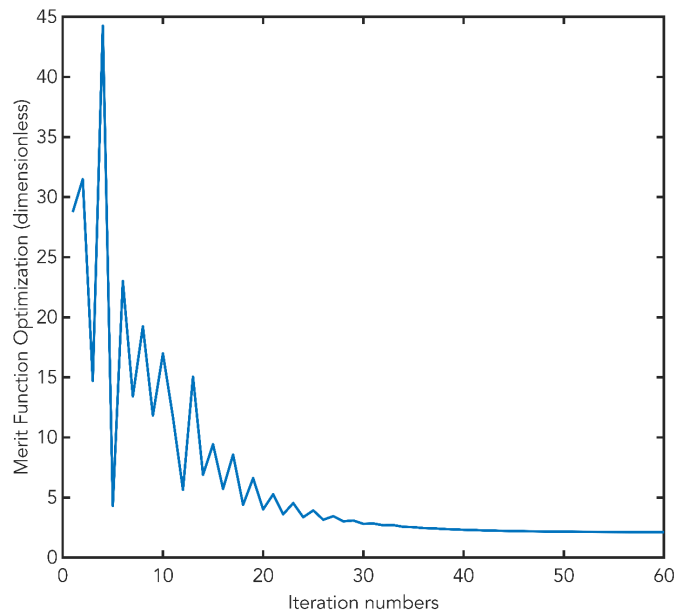
355 Fig. 10(b) and Fig 10(c) show the calculated damage factor  $H_{dm}$  value of the  $PK$  for each pixel and the  
 356  $H_{dm}$  value of the D65 illuminant for each pixel respectively. The results show that the damage factor with the  
 357 illuminant D65 is much greater than with the optimized light projection system developed in the investigation.



358 **Fig. 10. MF results.** (a) Shows the color difference,  $\Delta E_{00}$ , for each pixel of the printed picture  $AC_2$  illuminated by  
 359 light projection system and  $AC_1$  illuminated by reference illuminant D65. (b) Optimized  $H_{dm\_PK}$  for each pixel with  
 360 the light projection system developed (in  $Whm^{-2}$ ). (c) Calculated  $H_{dm\_d65}$  for each pixel for D65 illumination ( $Whm^{-2}$ )  
 361  $^2$ ), where  $H_{dm}$  (damage factor) is the effective irradiance that causes damage, which takes into account the  
 362 spectrum of incident radiation and the relative spectral response of the receiving material for one hour.  
 363

364 The optimization algorithm used two objective functions (color difference,  $\Delta E_{00}$ , and damage factor,  $H_{dm}$ ).  
365 The optimization algorithm used two objective functions (color difference,  $\Delta E_{00}$ , and damage factor,  $H_{dm}$ ).  
366 The optimization algorithm minimized the effective irradiance,  $H_{dm}$ , and color differences within 40 iterations.  
367 The MF implemented is a very flexible tool, as only a small change in the value of the weights is needed to  
368 modify the characteristics of the light projection system. An increase in weight directly increases the  
369 importance of the selected variable. In the optimization process used here, the quality of the color  
370 appearance was given a greater weight than damage ( $w_{\beta 1}=0.8$  and  $w_{\beta 2}=0.2$ ) to decrease color differences.

371 Figure 11 shows the results of the average merit function for all the pixels, based on the optimization  
372 iterations for damage and color difference caused by the illumination, optimized for *PK*. It has been verified  
373 that increasing the number of iterations does not improve the performance of the developed light projection  
374 system. The recommended number of iterations was  $n=40$ , since there were no improvements with  
375 additional iterations. This has been tested by increasing the number of iterations (e.g., 60, 70) and no  
376 appreciable decrease in the color difference or damage was been detected.



377  
378 **Fig. 11. MF iterations.** The average damage and color difference for all the pixels of the printed picture, as a  
379 function of iteration number. The merit function continues to improve the performance of the light projection  
380 system up to iteration 35, on average. Therefore, 40 iterations were performed for each pixel.

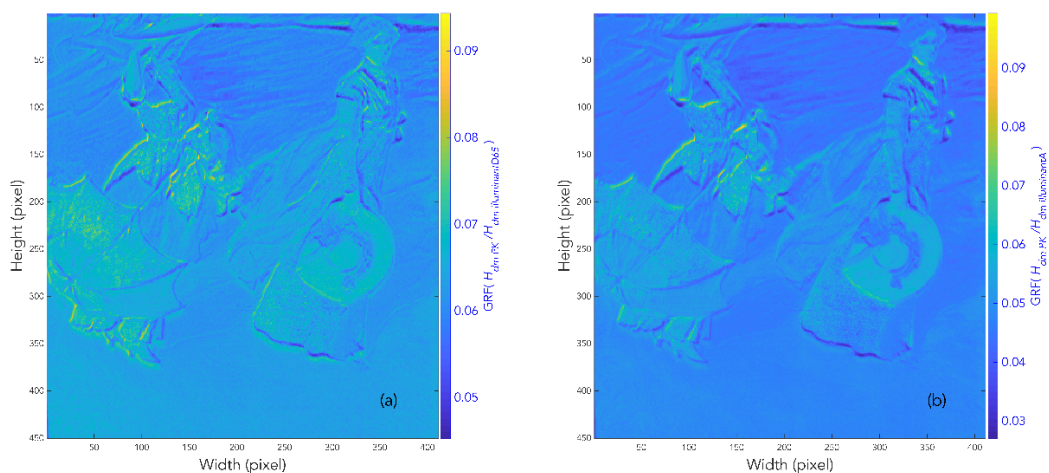
### 381 3.3 Damage by optical radiation

382 Since the Berlin Model recommended by CIE 157 (CIE 2004) does not fully capture the relationship  
383 between spectral reflectance and damage, relative light absorption calculations were performed to quantify  
384 the damage caused by light absorption. To develop a complete understanding of damage produced by light,  
385 the both the Berlin Model and a relative light absorption ( $\delta_{relative}$ ) have been considered in the results.

386 The light absorbed by each pigment under optimized lighting was compared to the amount of light  
387 absorbed when illuminated by reference daylight and incandescent illuminants. A reference standard D65  
388 illuminant was used in the color difference calculations to account for the lighting condition under which the  
389 artist created the painting (daylight). Incandescent was also used to calculate light absorption, since 51%  
390 of museums still use incandescent as the primary light source (Perrin, Druzik et al. 2014).

391 The damage factor ( $H_{dm}$ ) of the Berlin Model was used to calculate the relative damage to an oil painting  
392 represented by the printed picture. The average was  $H_{dm\_PK}=0.0185 \text{ Whm}^{-2}$  and the maximum was  
393  $H_{dm\_PK}=0.0312 \text{ Whm}^{-2}$  when the picture was illuminated by the light projection system, as shown in Fig.  
394 10(b). The average value was  $H_{dm\_D65}=0.2953 \text{ Whm}^{-2}$ , with a maximum of  $H_{dm\_D65}=0.4351 \text{ Whm}^{-2}$  when  
395 illuminated by D65, as shown in Fig. 10(c). When lit by illuminant A, the average value was  $H_{dm\_illuA}=0.3891$   
396  $\text{Whm}^{-2}$  and the maximum was  $H_{dm\_illuA}=0.5907 \text{ Whm}^{-2}$ .

397 Figure 12 shows the GRF of the effective radiation from the projector compared to the two illuminants.  
398 The light projection system developed optimizes the projected SPD by taking into account absorbed energy  
399 and damage factor ( $H_{dm}$ ). In this example, it has an average value that is 0.063 times the value for D65  
400 illumination, as shown in Fig. 12(a), and 0.0483 times the value for illuminant A, as shown in Fig. 12(b).



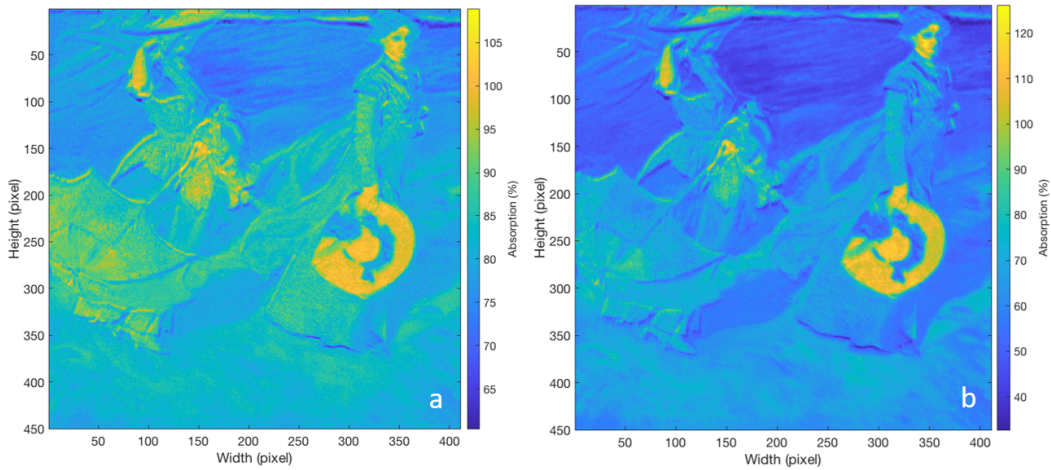
401  
402 **Fig. 12. GRF for optimized lighting compared to reference illuminants.** Shows the GRF when the printed  
403 picture is illuminated with the projector compared to the D65 illuminant, both with the same illuminance (100

404 cd/m<sup>2</sup>). (b) Shows the GRF for the same picture illuminated with the projector compared to illuminant A, both  
 405 with the same illuminance (100 cd/m<sup>2</sup>). Both figures show that the absorbed energy is much higher with  
 406 standard illuminants than when lit by the system developed here.

407 When it is not possible to measure the spectral responsivity function of the materials, the damage  
 408 evaluation must be applied without the reflectance information,  $S(\lambda)$ . In order to do this, relative light  
 409 absorption ( $\delta_{relative}$ ) is calculated

$$410 \quad \delta_{relative} = \frac{\int S_{test(x,y)}(\lambda)(1-\rho(\lambda)_{(x,y)})d\lambda}{\int S_{ref}(\lambda)(1-\rho(\lambda)_{(x,y)})d\lambda}, \quad (18)$$

411 where  $S_{test(x,y)}(\lambda)$  is the optimized SPD for each pixel,  $S_{ref}(\lambda)$  is the SPD of the reference daylight illuminant,  
 412 and  $\rho(\lambda)_{(x,y)}$  is the spectral reflectance factor of each pixel. The amount of light reflected (weighted by the  
 413 spectral luminous efficiency function) from the test and reference conditions were kept equal to prevent  
 414 color appearance phenomena, such as the Hunt effect (colorfulness increase with luminance) (Hunt 1952)  
 415 and the Bezold-Brucke hue shift (hue shift with luminance) (Pridmore 1999), and to ensure that reductions  
 416 in light absorption were not the consequence of reduced painting brightness.



417 **Fig. 13. Relative light absorption.** (a) The amount of light absorbed by each pixel of the printed copy picture  
 418  $\delta_{relative(x,y)}$  ranged from 61 % to 109 % under optimized lighting conditions, compared to the reference D65  
 419 illuminant. (b) The amount of light absorbed by each pixel ranged from 33 % to 126 % compared to the  
 420 reference incandescent illuminant.  
 421

422 The amount of light absorbed by the printed copy picture ranged from 61 % to 109 %, compared to the  
 423 reference daylight illuminant, as shown in Fig. 13(a). The average  $\delta_{relative}$  was 82 %, with a standard  
 424 deviation of 6 %. The amount of light absorption under the optimized SPD increased for only 2,113 pixels  
 425 (out of 450 x 411 pixels), comprising approximately 1 % of the image.

426 When the reference illuminant was incandescent, light absorption ranged from 33 % to 127 %. The  
427 average  $\delta_{relative}$  was 63 %, with a standard deviation of 12 % (Fig. 13(b)). The amount of light absorption  
428 under the optimized SPD increased for only 4,683 pixels (out of 450 x 411 pixels), which is around 2.5 %  
429 of the image.

#### 430 **4. Discussion**

431 This paper presents a methodology to enable non-invasive photonic restoration to obtain the best lighting  
432 for minimizing damage and maximizing color reproduction of a work of art, using a point by point spectral  
433 projection system. This methodology is tested on a printed picture, but it can also be implemented on  
434 different types of photoresponsivity medium (e.g., oil paintings, drawings, textiles, etc.).

435 The color degradation was simulated by a computer application to enable comparison to previous studies  
436 (Mayorga, Vazquez et al. 2016) and propose a complete methodology for developing a light projection  
437 system that visually restores the color of works of art with light. This example demonstrates that the  
438 proposed light projection system can alter the color of the printed picture  $AC_2$ , resulting in a virtual photonic  
439 restoration, yielding an excellent reproduction of non-aged printed picture  $AC_1$ .

440 This proposal is largely intended for application to certain specific cases in which most classic restoration  
441 techniques cannot be used. It has been demonstrated that the developed light projection system works  
442 correctly in the laboratory, with appreciable results, both in the improvement of the color appearance and in  
443 the reduction of the damage caused by the radiation. Nevertheless, this work must be improved for in situ  
444 applications, where it would be necessary to consider the art medium, its location, and to use more complex  
445 light sources than an RGB system. Additionally, more research is needed to develop a more comprehensive  
446 damage factor metric.

447 However, the proposed light projection system is functional and applicable, and its investment can be  
448 assumed if compared with the benefits that entail. The goal is to reach the works of art affected by a loss of  
449 color, where restorers and conservators do not recommend the use of invasive techniques because the  
450 advantages do not outweigh the damage caused. Another benefit that is achieved with this system is to  
451 delay further deterioration produced by lighting sources. The group has obtained a grant to implement this  
452 for a real picture from Dali entitled "Dos Figuras" and demonstrate it in Museo Reina Sofía in Madrid.

453 Although the calculations made involved in the process take time – in this example, given the size and  
454 resolution of the printed picture, it took approximately four hours – this aspect wouldn't meaningfully increase  
455 costs, since the calculations are only performed operation once and are automated.

456 The methodology used is transferable, with the necessary adaptations, to the personnel responsible for  
457 conservation in museums and art exhibitions, so that they can develop light projection systems adapted to  
458 the needs of particular works of art.

## 459 **5. Conclusions**

460 Degraded artwork can be photonic virtually restored using the proposed algorithms and hardware set-  
461 up. The damage caused to a work of art by optical radiation can be reduced by spectrally optimizing the  
462 light source emission.

463 Colorimetric calculations show that shifts in the color appearance of the non-damaged multi-colored  
464 painting under the reference daylight illuminant and the artificially damaged picture under optimized lighting  
465 conditions were imperceptible ( $\Delta E_{00\_PK}=0.27$ ), where  $\Delta E_{00}=1$  is a just-noticeable difference (JND) under  
466 controlled laboratory conditions. The amount of light absorbed by the painting, which could cause damage,  
467 was also reduced up to 40 % compared to a daylight illuminant and reduced up to 67 % when compared by  
468 an incandescent lamp.

469 These results show that a point-by-point optimized light projection system can substantially reduce  
470 damage to artwork and a decrease in energy consumption. Although the optimization algorithm minimizes  
471 the damage using the damage factor, it can be estimated that the light absorbed by the image of the printed  
472 copy, according to the reference studies, continues to cause damage. Absorption-minimizing light projection  
473 systems can offer a breakthrough in artwork conservation by preserving and virtually restoring artwork non-  
474 invasively.

## 475 **Funding source**

476 This research was supported by project RTI2018-097633-A-I00 from the Spanish Ministry funding  
477 “*Proyectos I+D Retos de Investigación*” entitled Photonic restoration applied to cultural heritage: application  
478 to Dali's picture “Dos Figuras”.

## 479 **Research Data**

480 Supplementary material associated with this article can be found, in the online version, at  
481 [doi:10.17632/n8wzw5fpx.1](https://doi.org/10.17632/n8wzw5fpx.1)

482 **6. References**

- 483 Al-Sallal, K. A., A. R. AbouElhamd and M. B. Dalmouk (2018). "UAE heritage buildings converted into  
484 museums: Evaluation of daylighting effectiveness and potential risks on artifacts and visual comfort."  
485 Energy and Buildings **176**: 333-359.
- 486 Bay, H., A. Ess, T. Tuytelaars and L. Van Gool (2008). "Speeded-up robust features (SURF)." Computer  
487 vision and image understanding **110**(3): 346-359.
- 488 Berns, R. S. (2011). "Designing white-light LED lighting for the display of art: A feasibility study." Color  
489 Research & Application **36**(5): 324-334.
- 490 Berns, R. S. (2019). "Digital color reconstructions of cultural heritage using color - managed imaging and  
491 small - aperture spectrophotometry." Color Research & Application: 16.
- 492 Bouguet, J. (2012). Camera calibration toolbox for Matlab. . Computational vision at the California institute  
493 of technology.
- 494 Capel, D. and A. Zisserman (2003). "Computer vision applied to super resolution." IEEE Signal  
495 Processing Magazine **20**(3): 75-86.
- 496 Chane, C. S., A. Mansouri, F. S. Marzani and F. Boochs (2013). "Integration of 3D and multispectral data  
497 for cultural heritage applications: Survey and perspectives." Image and Vision Computing **31**(1): 91-102.
- 498 CIE (2004). 157:2004 Control of damage to museum objects by optical radiation, CIE Commission  
499 Internationale de L'Eclairage Technical Report: 35.
- 500 CIE (2004). CIE 15:2004 Colorimetry.
- 501 Cuttle, C. (1996). "Damage to museum objects due to light exposure." Lighting Research and Technology  
502 **28**(1): 1-9.
- 503 De-Graaf, T., D. Mennatalla and M. I. Helmut (2013). "Sustainable lighting of museum buildings."  
504 Renewable Energy(0): --.
- 505 de Luna, J. M., D. V. Molini, A. A. Fernandez-Balbuena, A. G. Botella, J. A. Herraiez and R. Ontañon  
506 (2015). "Selective Spectral LED Lighting System Applied in Paleolithic Cave Art." LEUKOS **11**(4): 223-  
507 230.
- 508 Delgado, M. F., C. W. Dirk, J. Druzik and N. WestFall (2011). "Lighting the world's treasures: Approaches  
509 to safer museum lighting." Color Research & Application **36**(4): 238-254.
- 510 Durmus, D., D. Abdalla, A. Duis and W. Davis (2018). "Spectral optimization to minimize light absorbed by  
511 artwork." Leukos: 1-10.
- 512 Durmus, D. and W. Davis (2015). Absorption-Minimizing Spectral Power Distributions. Light, Energy and  
513 the Environment 2015, Suzhou, Optical Society of America.

- 514 Durmus, D. and W. Davis (2015). "Optimising light source spectrum for object reflectance." Optics express  
515 **23**(11): A456-A464.
- 516 Durmus, D. and W. Davis (2017). "Object color naturalness and attractiveness with spectrally optimized  
517 illumination." Optics Express **25**(11): 12839-12850.
- 518 Fairchild, M. D. (2013). Color appearance models. Chichester, West Sussex, England, John Wiley &  
519 Sons.
- 520 Fechner, G. (1860). "1966. Elements of psychophysics." Elements of Psychophysic. 1st Ed. New York,  
521 NY: Holt, Rinehart, and Winston Inc.
- 522 Fernandez-Balbuena, A. A., M. Gonzalez, A. Garcia-Botella and D. Vazquez-Molini (2015). "Application of  
523 dynamic merit function to nonimaging systems optimization." Optical Engineering **54**(2): 025107.
- 524 G. Sharma, W. W., EN. Dalal (2005). "The CIEDE2000 color-difference formula: Implementation notes,  
525 supplementary test data, and mathematical observations." Color Research & Application **30**(1): 21--30.
- 526 Hecht, J. (2015). "Light repairs art: optical overlays restore faded masterworks." Optics and Photonics  
527 News **26**(4): 40-47.
- 528 Hilbert, G., S. Aydinli and J. Krochmann (1991). "Zur Beleuchtung musealer Exponate: Neuere  
529 konservatorische Erkenntnisse." Restauro **97**(5): 313-321.
- 530 Hunt, R. W. G. (1952). "Light and dark adaptation and the perception of color." JOSA **42**(3): 190-199.
- 531 Hwang, S., H. Song, S.-W. Cho, C. E. Kim, C.-S. Kim and K. Kim (2017). "Optical measurements of  
532 paintings and the creation of an artwork database for authenticity " PLoS ONE **12**(2): 1-14.
- 533 Imai, F. H., M. R. Rosen and R. S. Berns (2000). Comparison of spectrally narrow-band capture versus  
534 wide-band with a priori sample analysis for spectral reflectance estimation. Color and Imaging  
535 Conference, Society for Imaging Science and Technology.
- 536 Lagarias, J. C., J. A. Reeds, M. H. Wright and P. E. Wright (1998). "Convergence Properties of the  
537 Nelder–Mead Simplex Method in Low Dimensions." SIAM Journal on Optimization **9**(1): 112-147.
- 538 Lin, W. C., T. S. Huang, T. C. Ho, Y. T. Chen and J. H. Chuang (2013). Interactive lighting design with  
539 hierarchical light representation. Computer Graphics Forum, Wiley Online Library.
- 540 Marimont, D. H. and B. A. Wandell (1992). "Linear models of surface and illuminant spectra." Journal of  
541 the Optical Society of America A **9**(11): 1905-1913.
- 542 Mayorga, S., D. Vazquez, A. A. Fernandez-Balbuena, G. Hernandez, J. A. Herraes, M. Azcutia and A.  
543 Garcia (2016). "Advanced daylighting evaluation applied to cultural heritage buildings and museums:  
544 Application to the cloister of Santa Maria El Paular." Renewable Energy **85**: 1362-1370.
- 545 Mayorga, S., D. Vazquez, A. A. Fernandez-Balbuena, C. Muro and J. Muñoz (2016). "Spectral damage  
546 model for lighted museum paintings: Oil, acrylic and gouache." Journal of Cultural Heritage **22**: 931-939.

- 547 Michalski, S. (2013). "Agent of deterioration: light, ultraviolet and infrared." Ottawa: Canadian  
548 Conservation Institute. Last modified 6.
- 549 Miller, J. V. (1993). Evaluating Fading Characteristics of Light Sources, NoUVIR Research.
- 550 Mueller, H. F. (2013). "Energy efficient museum buildings." Renewable energy **49**: 232-236.
- 551 Murakami, Y., M. Yamaguchi and N. Ohyama (2012). "Hybrid-resolution multispectral imaging using color  
552 filter array." Optics express **20**(7): 7173-7183.
- 553 Nelder, J. and R. Mead (1965). "A simplex method for function minimization." The computer journal **7**(4):  
554 6.
- 555 Pavlogeorgatos, G., 2003. Environmental parameters in museums. Build. Environ. **38**, 1457–1462.
- 556 Perrin, T., J. Druzik and N. Miller (2014). SSL adoption by museums: survey results, analysis, and  
557 recommendations, Pacific Northwest National Lab.(PNNL), Richland, WA (United States).
- 558 Phillips, D. C. (1912). "Sorolla: the Painter of Sunlight." Art and Progress: 791-797.
- 559 Pridmore, R. W. (1999). "Bezold–Brucke hue-shift as functions of luminance level, luminance ratio,  
560 interstimulus interval and adapting white for aperture and object colors." Vision research **39**(23): 3873-  
561 3891.
- 562 Quiroga, J. A., J. Zoido, J. Alonso and E. Bernabeu (1994). "Colorimetric matching by minimum-square-  
563 error fitting." APPLIED OPTICS Optical Society of America **33**(26): 3.
- 564 Saunders, D. and J. Kirby (1994). "Wavelength-dependent fading of artists' pigments." 190--194.
- 565 Schaeffer, T. T. (2002). Effects of light on materials in collections: data on photoflash and related sources.  
566 Los Angeles, Getty Publications.
- 567 Schanda, J. (2007). Colorimetry. Understanding CIE System, John Wiley & Sons.
- 568 Shen, H. L., P. Q. Cai, S. J. Shao and J. H. Xin (2007). "Reflectance reconstruction for multispectral  
569 imaging by adaptive Wiener estimation." Optics express **15**(23): 15545-15554.
- 570 Simpson, M. L. and J. F. Jansen (1991). "Imaging colorimetry: a new approach." Applied Optics **30**(32):  
571 4666-4671.
- 572 Stenger, J., N. Khandekar, R. Raskar, S. Cuellar, A. Mohan and R. Gschwind (2016). "Conservation of a  
573 room: A treatment proposal for Mark Rothko's Harvard Murals " Studies in Conservation **61**(6): 348-361.
- 574 Viénot, F., G. Coron and B. Lavédrine (2011). "LEDs as a tool to enhance faded colours of museums  
575 artefacts." Journal of Cultural Heritage **12**(4): 431-440.

576 Vincent, E. and R. Laganière (2005). "Detecting and matching feature points." Journal of Visual  
577 Communication and Image Representation **16**(1): 38-54.

578 Zhang, Z. (2000). "A flexible new technique for camera calibration." IEEE Transactions on pattern analysis  
579 and machine intelligence **22**(11): 1330-1334.

580

581